Characterization of Microcellular Biodegradable Polymeric Foams Produced from Supercritical Carbon Dioxide Solutions

S. Cotugno, E. Di Maio, and G. Mensitieri*

Department of Materials and Production Engineering University of Naples FEDERICO II, P. le Tecchio 80, 80125 Naples, Italy

S. Iannace

IMCB-CNR Institute for Composite and Biomedical Materials, P. le Tecchio 80, 80125 Naples, Italy

G. W. Roberts, R. G. Carbonell, and H. B. Hopfenberg

Department of Chemical Engineering, North Carolina State University, Raleigh, North Carolina 27695-7565

The formation of foams of biodegradable poly(ϵ-caprolactone) (PCL) from CO_2 solutions in molten PCL was investigated. This study included characterization of the CO_2 diffusion and equilibrium solubility in molten PCL in contact with supercritical CO_2 ($scCO_2$). Experiments were performed at 70, 80, and 90 °C at CO_2 pressures up to 25 MPa. The effective mutual diffusivity of CO_2 in molten PCL was measured as a function of the CO_2 pressure. The data revealed a dramatic increase in apparent effective diffusivity at elevated pressure, likely related to the formation of fluid bubbles, phase-separated from the previously homogeneous, molten PCL solution of CO_2. Microcellular PCL foams were produced by starting from an equilibrium CO_2−PCL solution at 70 °C over a wide range of initial pressures (from 6.9 to 32 MPa) by quenching down to foaming temperatures (from 24 to 30 °C) followed by rapid depressurization to atmospheric pressure. Foam structures were characterized by scanning electron microscopy, and cell sizes and density were determined quantitatively. The various foam structures were analyzed and interpreted in connection with the independently measured kinetics and equilibrium of CO_2 sorption in PCL by considering the effects of starting pressure and foaming temperature on bubble nucleation and growth.

1. Introduction

Foams are of particular interest in commercial applications, including packaging, acoustic and thermal insulation, biomedical products, and sporting equipment.[1−3] The foam density and cell size distribution influence the final properties of the foam. A foam with high density and relatively high tensile strength and Young's modulus can be used for structural parts, while low-density foams can be used in thermal and acoustic insulation as well as in packaging applications. The large and increasing volume of manufactured, foamed, polymeric materials has stimulated interest in developing useful innovations related to recycling the materials used in these high-volume applications.

An alternative to recycling is the use of biodegradable polymers, such as poly(ϵ-caprolactone) (PCL), as a foam matrix. The use of supercritical CO_2 ($scCO_2$) as a blowing agent is also useful in developing environmentally benign foaming processes. In fact, $scCO_2$ can be used as a substitute for traditional blowing agents that, in addition to environmental concerns, often compromise control of the final structure of the microcellular plastic. In fact, many traditional blowing agents belong to the class of chlorofluorocarbons (CFC), which are clearly recognized to contribute to serious effects on the ozone layer. As a result, CFC's were banned by the Montreal Protocol in 1987. Several studies over the past decade have shown the importance of $scCO_2$ in polymer processing, including foaming, coating, and additive impregnation.[3−9]

Microcellular foaming using CO_2 as a blowing agent has been reported in the literature for several polymers, e.g. polystyrene (PS), polyamide 11 (PA 11), and poly(methyl methacrylate) (PMMA).[1,3,10] For these systems, various models for homogeneous nucleation and growth of the bubbles in the gas−polymer mixture have been proposed.[5,11−14] The initial nucleation is induced by a change in temperature and/or pressure of the mixture. Once the bubble is nucleated, it will grow, due to the diffusion of the gas dissolved in the molten polymer to the nucleated bubble. In this respect, the nucleation and the growth of the bubble are related to sorption equilibria and mass transport kinetics of the blowing agent in the molten polymer as well as to the rheological and surface properties of the mixture surrounding the bubble itself.[9,13]

This study focuses upon interpreting the effects of the kinetics and equilibria of sorption of CO_2 in PCL on the nature of the PCL foams produced from $scCO_2$. The equilibrium sorption has been determined at 70, 80, and 90 °C at pressures up to 25 MPa, and data have been analyzed using the Sanchez−Lacombe (SL) lattice model[15−18] and the Peng−Robinson equation of state (PR-EOS).[19] In fact, the equilibrium concentration of CO_2 in PCL, at each temperature and pressure, has been evaluated by equating the chemical potential of

* To whom correspondence should be addressed. Phone: +39 081 7682512. Fax: +39 081 7682404. E-mail: mensitie@unina.it.

10.1021/ie049445c CCC: $30.25
Published on Web 02/19/2005

Table 1. Physical Properties of PCL

wt av mol wt (M_w)	glass transition temp (T_g)	melting temp (T_m)	crystallizn temp (T_{cry})
80 000	−60 °C	60 °C	27.4 °C

CO_2 in the polymeric mixture and in the contiguous fluid phase, assumed to be in equilibrium with the molten polymeric phase. The chemical potential of CO_2 in the polymer phase was calculated using the SL model, while the chemical potential of CO_2 in the fluid phase was calculated using the PR-EOS. The latter approach has been adopted, since Peng−Robinson equations are expected to provide a more reliable predictive capability than SL theory in the supercritical range of CO_2.

We explored the possibility of obtaining microcellular foams by using a batch foaming technique based on $scCO_2$ as a blowing agent. The effects of initial equilibrium pressure (in the 6.9−32 MPa range and at 70 °C) and of foaming temperature (in the 24−30 °C range and at an initial equilibrium pressure equal to 6.9 MPa) on the final structure of the foam have been studied.

2. Experimental Section

2.1. Materials. Poly(ϵ-caprolactone) was supplied by Solvay Interox Ltd. (PCL CAPA 6800). The physical properties of the PCL are presented in Table 1.

The parameters of SL-EOS for pure PCL, determined by fitting PVT data at pressures up to 50 MPa and temperatures from 70 to 120 °C, are[20]

$$P_2^* = 548.6 \text{ MPa}$$

$$T_2^* = 637.7 \text{ K}$$

$$\rho_2^* = 1.158 \text{ g/cm}^3$$

From these parameters, the *close-packed* mer volume[18] can be calculated:

$$v_2^* = \frac{RT_2^*}{P_2^*} = 9.66 \text{ cm}^3/\text{mol}$$

The liquid carbon dioxide (bone dry grade 2.8, purity >99.8%) was obtained from National Welders NC and used as received. The parameters of SL-EOS for pure CO_2 were taken from the literature:[21,22]

$$P_1^* = 574.5 \text{ MPa}$$

$$T_1^* = 305.3 \text{ K}$$

$$\rho_1^* = 1.510 \text{ g/cm}^3$$

From these values, we obtain

$$v_1^* = \frac{RT_1^*}{P_1^*} = 4.42 \text{ cm}^3/\text{mol}$$

$$r_1^0 = \frac{M_1}{\rho_1^* v_1^*} = 6.60$$

where M_1 is the molecular weight of carbon dioxide and r_1^0 is the number of lattice sites occupied by a carbon dioxide molecule. Here and in the following, subscripts 1 and 2 will refer respectively to carbon dioxide and PCL.

2.2. Methods. 2.2.1. CO_2 Sorption Measurement. The sorption equilibrium and mass transport behavior were studied using a quartz spring microbalance and a magnetic suspension balance. All the experiments were performed above the melting temperature of neat PCL and well above its glass transition temperature. The quartz spring balance was used to provide carbon dioxide sorption data in the low-pressure range (0−7 MPa) at 70 °C, while the magnetic suspension balance was used at 70, 80, and 90 °C in the high-pressure range, 0−25 MPa. These high-pressure values can be attained due to the particular electromagnetic coupling between the balance mechanism and the freely suspended measuring load, which allows the physical separation of the balance from the measuring chamber.

Sorption experiments were conducted by measuring changes of sample weight with a calibrated quartz spring microbalance (RUSKA Co., Houston, TX; maximum elongation 400 mm, maximum weight 50 mg) placed in a pressurized stainless steel cylindrical vessel (2.54 cm diameter) equipped with high-pressure viewing ports and with a water jacket for accurate temperature control. The polymer sample was placed in an aluminum pan (which guaranteed dimensional stability of the sample) and hung on the lower spring hook. The aluminum pan had a cylindrical shape, and its dimensions were accurately measured. The initial thickness of the molten polymer was estimated by knowing its density at the temperature of interest (as calculated from PVT measurements), the weight of the sample, and the diameter of the pan. The kinetics of CO_2 sorption and sorption equilibrium values in the molten polymer were evaluated by measuring spring elongation with a traveling microscope (resolution of 0.01 mm). To ensure the measurement of the absolute spring elongation, an undeformable reference glass rod, coaxial to the spring helix, was used.

Measurements were conducted by performing step-change sorption experiments. Consecutive sorption tests were conducted by step increments of the carbon dioxide pressure (about 0.3 MPa steps) with preheated carbon dioxide, after the attainment of equilibrium sorption in the previous step.

When penetrant diffusivity is expected to depend on penetrant concentration, data should be properly analyzed to derive meaningful diffusion coefficients from step-change experiments. In this investigation we adopted a method proposed by Vrentas et al.[23] to obtain the value of mutual diffusivity, $D(C)$, at a specific penetrant concentration, C, between the initial and final concentrations of each sorption experiment. The method is based on the evaluation of an average mutual diffusivity ($\bar{D}$) from the initial rate of sorption. Since the system under investigation follows a Fickian behavior, the expression for $\bar{D}$ takes the form[24]

$$\bar{D} = \frac{\pi L^2}{4}\left(\frac{\mathrm{d}(M_t/M_\infty)}{\mathrm{d}(\sqrt{t})}\right)^2 \qquad (1)$$

where M_t is the mass of carbon dioxide sorbed at time t, M_∞ is the amount sorbed at equilibrium, and L is the sample thickness (sample is exposed to the gas phase on one side only). The value of $\bar{D}$ calculated through eq 1 corresponds to the value of the carbon dioxide mutual diffusivity, $D(C)$, at a certain concentration value which

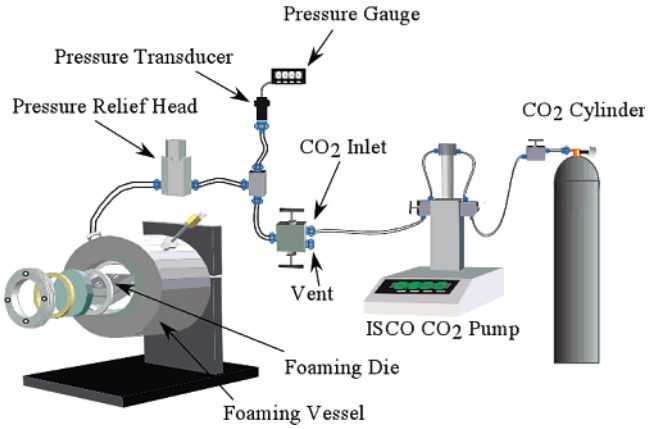

Figure 1. Batch foaming apparatus.

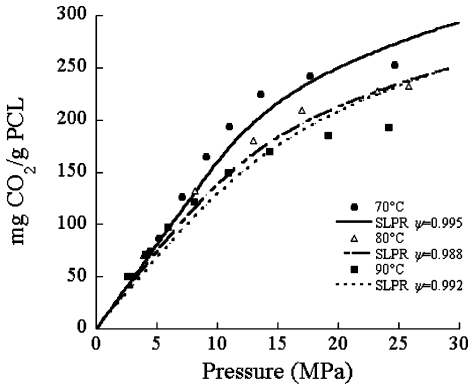

Figure 2. Sorption isotherms of CO_2 in PCL at 70, 80, and 90 °C: comparison between experimental data determined using a Rubotherm apparatus and the best fitting performed using SL-PR EOS. The label reports best-fitting values for ψ.

can be evaluated following the procedures proposed by Vrentas et al.[23] Since the sample volume increased with carbon dioxide concentration, for each sorption step the sample thickness to be used in the analysis of the data was estimated from the mixture volume predicted by the SL equation of state (SL-EOS), using the arithmetic average of initial and final density of the polymer−gas mixture.

A buoyancy correction was also performed, consistent with the carbon dioxide density and the volumes of the sample (as evaluated from SL-EOS), the pan, and the spring. The volumes of the pan and the spring have been previously determined by evaluating the buoyancy effect at test conditions but without the polymer sample.

In the case of the magnetic suspension balance measurements (Rubotherm ISOSORP, Bochum, Germany, maximum weight 100 g, resolution 10 μg), a crucible containing the polymer sample was attached to a permanent magnet. The system was placed in a sorption chamber maintained at a controlled temperature (±0.05 °C). The system could withstand pressures up to 30 MPa. The permanent magnet was kept suspended by an electromagnet, which was attached to the hook of an analytical balance (SARTORIUS Model MC 5). Coupling between the magnet and the electromagnet was controlled electronically. The balance and the electromagnet were completely isolated from the sorption chamber and maintained at ambient conditions. The force change due to mass uptake during the sorption process was transmitted from the sorption chamber to the analytical balance by the coupling of the permanent magnet and electromagnet. The experimental protocol used to determine diffusion coefficients and sorption equilibria were similar to those used in the quartz spring microbalance experiments. The pressure of $scCO_2$ in the sorption chamber was controlled by means of a high-pressure syringe pump (Isco 500D). The balance is also equipped with a system for the automatic, continuous evaluation of the density of the $scCO_2$ in the measuring chamber, based on the buoyancy effect on a known weight. Sorption isotherms were determined by using both the Rubotherm and quartz spring systems at each temperature and are reported as equilibrium sorption values as a function of pressure.

2.2.2. Description of Batch Foaming Protocol. The preparation of foam samples was carried out in a thermoregulated and pressurized 316 SS high-pressure cylindrical cell (see Figure 1). Typical experiments were conducted using the following procedure. A known mass of PCL was charged into the cell, which was then purged with carbon dioxide under ambient conditions. The temperature was raised to 70 °C, 10 °C above the melting temperature of pure PCL, and the cell was filled with CO_2 at the desired pressure (referred in the following as initial pressure, P_{IN}) by using an ISCO pump (Isco 500D). Molten polymer samples were kept under these conditions ($P = P_{IN}$ and $T = 70$ °C) for around 4 h: that is, a contact time sufficient to achieve sorption equilibrium in view of the thickness (around 2 mm) of the adopted molten samples. The cell temperature was then dropped to the foaming temperature, T_{FOAM}, equal to 24, 27, or 30 °C, in about 5 min. The cell was then vented by dropping the pressure to 1 atm in around 4 s. This venting time is referred to in the following as foaming time, t_{FOAM}. Several batch foaming experiments were performed at different values of P_{IN}, in the range 6.5−32 MPa.

2.2.3. Scanning Electron Microscopy. The foamed samples were sectioned in liquid nitrogen and coated with gold using a sputter coater. The structure, revealed by the examination of the fracture surface, was determined by using a variable-pressure scanning electron microscope (Hitachi S3200N VP-SEM).

3. Results and Discussion

3.1. $scCO_2$ Sorption Isotherms in Molten PCL. The sorption isotherms were determined using the two experimental techniques. The Rubotherm apparatus was used over the pressure range 0−25 MPa at 70, 80, and 90 °C, and the quartz spring balance was used over the pressure range 0−7 MPa at 70 °C. The results are shown in Figures 2 and 3, respectively.

Sorption equilibrium data were interpreted using the SL and PR-EOS. In particular, at each temperature and pressure, the equality of molar Gibbs free energy of CO_2 in the gaseous phase and in the molten polymer mixture has been imposed:

$$G_1(T, P) = \bar{G}_1^{M}(T, P) \tag{2}$$

where G_1 is the molar free energy of carbon dioxide in the pure gaseous phase and $\bar{G}_1^{M}$ is the partial molar free energy of carbon dioxide in the polymer mixture (it is assumed here that polymer chains are not dissolved in the carbon dioxide rich phase). Using as a reference the molar free energy of the ideal gas ("IG")

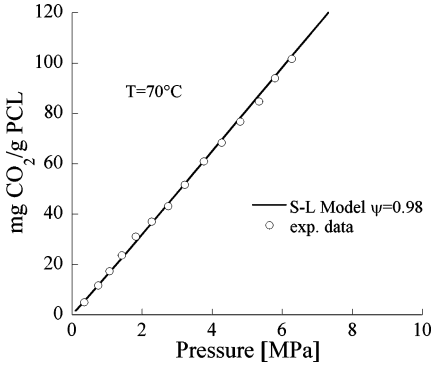

Figure 3. Sorption isotherm data of CO_2 in PCL at 70 °C: comparison between experimental data determined using a Quartz spring apparatus and the best fitting performed using SL-PR EOS. The label reports the best-fitting value for ψ.

at the temperature of interest and at $P = 1$ atm (in the following P_{atm}), eq 2 becomes

$$G_1(T,P) - G_1^{IG}(T,P_{atm}) = \bar{G}_1^{M}(T,P) - G_1^{IG}(T,P_{atm}) \quad (3)$$

On the basis of the definition of fugacity, f, of a real gas, it is readily found that the left-hand side of eq 3 is equal to

$$\frac{G_1(T,P) - G_1^{IG}(T,P_{atm})}{RT} = \ln(f_1/P_{atm}) \quad (4)$$

Using the PR-EOS the right-hand side of eq 4 can be expressed as

$$\ln(f_1/P_{atm}) = \ln(P/P_{atm}) + Z - 1 - \ln(Z-B) - \frac{A}{2\sqrt{2}B}\ln\left(\frac{Z+2.414B}{Z-0.414B}\right) \quad (5)$$

Terms in the above expressions are defined as

$$A = \frac{aP}{R^2T^2}$$

$$B = \frac{bP}{RT}$$

$$Z = \frac{Pv}{RT}$$

where P is the pressure, T the temperature, v the specific volume of the gas, and R the gas constant. The parameters a and b in the above expressions are

$$a(T) = [a(T_c)][\alpha(T/T_c, \omega)]$$

$$b(T) = b(T_c)$$

with

$$a(T_c) = 0.457\,24\frac{R^2T_c^{\,2}}{P_c}$$

$$b(T) = 0.077\,80\frac{RT_c}{P_c}$$

$$\alpha^{1/2} = 1 + \kappa[1 - (T/T_c)^{1/2}]$$

$$\kappa = 0.374\,64 + 1.542\,26\omega = 0.269\,92\omega^2$$

where T_c and P_c are, respectively, the critical temperature and pressure of the fluid phase and ω is the acentric factor.[19] The CO_2 specific volume, v, which is needed to evaluate Z, has been calculated using the PR-EOS:

$$P = \frac{RT}{v-b} - \frac{a(T)}{v(v+b)+b(v-b)}$$

The right-hand side of eq 3 has been evaluated using the SL theory[18] for both the mixture and pure carbon dioxide at P_{atm}:

$$\frac{\bar{G}_1^{M}(T,P) - G_1^{IG}(T,P_{atm})}{RT} = \ln\phi_1 + \phi_2 + \tilde{\rho}r_1^{0}X_1\phi_2^{\,2} + \left[-\frac{\tilde{\rho}}{\tilde{T}_1} + \frac{\tilde{P}_1}{\tilde{T}_1\tilde{\rho}} + \frac{(1-\tilde{\rho})\ln(1-\tilde{\rho})}{\tilde{\rho}} + \frac{\ln\tilde{\rho}}{r_1^{0}}\right]r_1^{0} - r_1^{0}\left[-\frac{\tilde{\rho}_1}{\tilde{T}_1} + \frac{\tilde{P}_1}{\tilde{T}_1\tilde{\rho}_1} + \frac{(1-\tilde{\rho}_1)\ln(1-\tilde{\rho}_1)}{\tilde{\rho}_1} + \frac{\ln\tilde{\rho}_1}{r_1^{0}}\right]\Bigg|_{P=P_{atm}} \quad (6)$$

Here, to evaluate $G_1^{IG}(T, P_{atm})$, it has been assumed that the carbon dioxide has an ideal gas behavior at the temperatures of interest and at P_{atm}.

The reduced density of the mixture, $\tilde{\rho}$, and the reduced density of carbon dioxide at P_{atm} ($\tilde{\rho}_1^{P_{atm}}$) to be used in the right-hand side of eq 6 were calculated using the SL-EOS:[18]

$$\tilde{\rho} = 1 - \exp\left[-\frac{\tilde{\rho}^2}{\tilde{T}} - \frac{\tilde{P}}{\tilde{T}} - \left(1 - \frac{\phi_1}{r_1}\right)\tilde{\rho}\right] \quad (7)$$

$$\tilde{\rho}_1 = 1 - \exp\left[-\frac{\tilde{\rho}_1^{\,2}}{\tilde{T}_1} - \frac{\tilde{P}_1}{\tilde{T}_1} - \left(1 - \frac{1}{r_1^{0}}\right)\tilde{\rho}_1\right] \quad (8)$$

In the above expressions, ϕ_1 and ϕ_2 represent the close packed volume fraction of the two components in the mixture, while r_1 represents the number of lattice sites occupied by a carbon dioxide molecule in the mixture.[18] The close-packed volume fraction of carbon dioxide in the polymer is related to the weight fractions (ω_1, ω_2) of the two components as follows:[18]

$$\phi_1 = \frac{\frac{\omega_1}{\rho_1^*}}{\frac{\omega_1}{\rho_1^*} + \frac{\omega_2}{\rho_2^*}}$$

while r_1 is related to r_1^0 by the equation

$$r_1 = \frac{r_1^{0}v_1^*}{v^*}$$

where v^* is the average close-packed volume of all mers in the mixture.

The reduced variables are defined by the expressions

$$\tilde{P} = P/P^*$$

$$\tilde{P}_1 = P/P_1^*$$

$$\tilde{T} = T/T^*$$

$$\tilde{T}_1 = T/T_1^*$$

$$\tilde{\rho} = \rho/\rho^*$$

$$\tilde{\rho}_1 = \rho_1/\rho_1^*$$

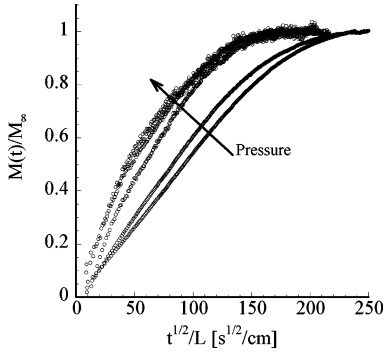

Figure 4. Sorption kinetics of CO_2 at various pressures in PCL at 70 °C obtained with a Rubotherm apparatus.

The mixture parameters are evaluated based on specific mixing rules:[18,25]

$$P^* = \phi_1 P_1^* + \phi_2 P_2^* - \phi_1 \phi_2 \Delta P^*$$

$$T^* = \frac{P^*}{\left(\frac{\phi_1 P_1^*}{T_1^*} + \frac{\phi_2 P_2^*}{T_2^*}\right)}$$

$$\rho^* = (\omega_1 \rho_1^* + \omega_2 \rho_2^*)^{-1}$$

The only parameter which characterizes the binary mixture is ΔP^* or X_1; these are defined as

$$\Delta P^* = P_1^* + P_2^* - 2P_{12}^*$$

$$P_{12}^* = \psi \sqrt{P_1^* P_2^*}$$

$$X_1 = \frac{\Delta P^* M_1}{RT \rho_1^* r_1^0}$$

where ψ is a dimensionless parameter which measures the deviation of P_{12}^* from the geometric mean.

A comparison between the prediction of the theoretical model (i.e. eqs 3−8) and the experimental data is shown in Figures 2 and 3. A best fit to the data was obtained by using as the fitting parameter the SL interaction parameter, ψ. Best-fit values are reported in the insets of Figures 2 and 3. A satisfactory agreement between the theoretical model and the experimental data was obtained over the pressure range 0−7 MPa, while significant deviations between the prediction of the model and the experimental data were observed over the pressure range 7−25 MPa.

3.2. Sorption Kinetics of scCO₂ in Molten PCL. Effective mutual diffusion coefficients of CO_2 in molten PCL were evaluated according to the procedure reported in the Experimental Section. Sorption kinetics obtained with the magnetic suspension balance for pressures comprised between 0.2 and 10 MPa, at 70 °C, are presented in Figure 4 as plots of $M(t)/M_\infty$ versus the square root of time divided by the thickness of the sample. At CO_2 pressures below its critical pressure ($P_c^{CO_2}$ = 7.38 MPa) the kinetics of carbon dioxide sorption in PCL exhibit essentially linear behavior up to a value of at least $M(t)/M_\infty$ equal to 0.6, consistent with purely Fickian diffusion. At higher pressures, the kinetics of sorption change significantly, most likely due to the formation of a dispersed fluid phase within the polymer at elevated pressures, discussed later.

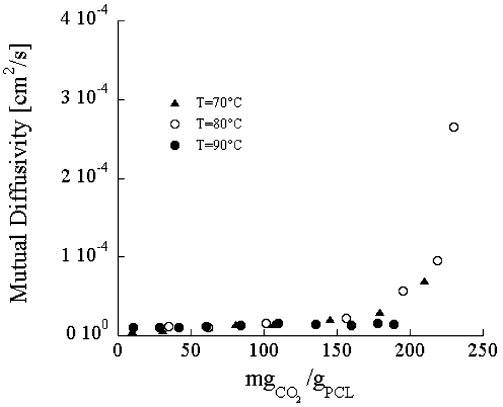

Figure 5. Mutual diffusivity of CO_2 in the PCL/CO_2 system vs carbon dioxide concentration in the polymer phase.

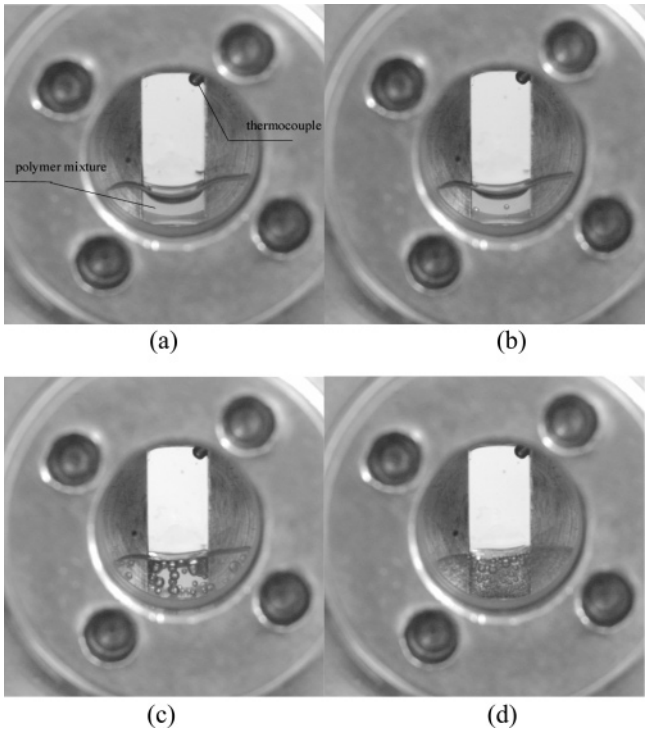

Figure 6. Photographs of the molten PCL/CO_2 system in the view cell at 70 °C and different pressures: (a) 3.45, (b) 6.80, (c) 13.80, and (d) 24.15 MPa.

The values of the mutual diffusion coefficient at 70, 80, and 90 °C and at pressures up to 25 MPa are reported in Figure 5 as a function of carbon dioxide concentration (mg_{CO_2}/g_{PCL}). A steady increase of $D(C)$ with CO_2 concentration occurs up to about 100 mg_{CO_2}/g_{PCL} while at higher values of concentration an apparent marked increase of the diffusivity occurs at 70 and 80 °C at pressure levels of CO_2 above $P_c^{CO_2}$. In fact, subsequent experiments performed at 70 °C using a view cell apparatus[26] showed that, at pressures above $P_c^{CO_2}$, bubble formation occurs in the polymer−scCO₂ mixture. In Figure 6 are reported photographs of the molten PCL/CO_2 system in the view cell taken at different pressures (3.45, 6.9, 13.8, and 24.15 MPa) at 70 °C. The observed increase of the effective mutual diffusivity at higher pressures is, therefore, consistent with the formation of a second, dispersed, low-density phase. Under these experimental conditions, CO_2 diffusion occurs in a heterogeneous medium, comprising bubbles

of fluid dispersed in the molten polymer−CO_2 solution, which provide a parallel, lower resistance path for diffusion.

The formation of a separate fluid phase in the bulk of the polymer-rich solution induced by pressure increase suggests rather peculiar phase bahavior of the system at hand. In fact, few examples have been reported in the literature of demixing of polymer−solvent mixtures induced by pressure increase, as, for example, the case of the cyclohexane−polystyrene and 1-phenyldecane−polystyrene systems.[27,28] Relevant examples are available also for the case of polymer solutions in supercritical fluids, as is the case of pressure-induced demixing upon an increase in pressure in polymer solutions of poly(dimethylsiloxane) in supercritical carbon dioxide[29] and of the anomalous swelling behavior of PMMA films exposed to supercritical CO_2.[30] The behaviors of polymer solutions in supercritical fluids are dominated by the large differences in free volume between solvent and polymer as well as by the isothermal compressibility, the volume expansivity, and concentration fluctuations of the solution. Energetic (enthalpy of mixing) and entropic thermodynamic forces (entropy of mixing and noncombinatorial entropy changes related to free volume dissimilarities between the solvent and the polymer) determine the phase behavior of the system. In particular, phase instability is determined by the relative importance of an "incompressible" contribution and a "compressible" contribution. The latter is scaled by the solution compressibility and always contributes unfavorably to phase stability.[30−32] In the case of PMMA thin films contacted with supercritical CO_2,[30] the authors report anomalous maxima in the swelling isotherms. Interestingly, these maxima occur in the regions of pressure/temperature where pure CO_2 compressibility also shows a maximum. This maximum in compressibility shifts to higher pressures and becomes broader and smaller in magnitude as the temperature increases: a consistent trend was observed also for the anomalous swelling maxima. This anomalous swelling was attributed to the formation of a less dense phase, due to a separation of CO_2 from the polymer as a consequence of decrease in CO_2 solubility promoted by an increase in compressibility. The phase-separated CO_2-rich phase does not leave the polymer film over the experimental time scale, due to reduced mobility of the surrounding polymer-rich phase and, as postulated by the authors, to critical wetting phenomena that allow the CO_2 to remain and expand the film.

Similar arguments can be invoked to justify also the phase separation behavior, induced by pressure increase, observed in the present investigation. Supercritical fluids are characterized by large gas compressibilities near the critical point, which can produce abrupt changes in density over small pressure increment. As a consequence also the "quality" of the solvent is greatly influenced by pressure and temperature conditions. Depending on the nature of the prevailing interactions in the system between solvent and polymer molecules (attractive or repulsive), the solvent quality can increase or decrease with increasing density (or, equivalently, pressure).[32] It is likely that at the temperature conditions considered in the present investigation the maxima in CO_2 compressibility, which are still relevant, play a role in affecting the phase behavior and inducing at 70 °C a phase separation evident from the visual inspection as well as from the abrupt increase of the apparent diffusivity. This phenomenon tends to decrease with temperature in connection with the broadening and with the decrement of the compressibility maximum, which moves toward higher pressures. A maximum in the sorption isotherms would be expected if the phase-separated fluid phase could completely separate from the polymer-rich phase. It is likely that, in the case under investigation, this effect was not observed, since the high viscosity of the surrounding medium and possible critical wetting phenomena prevent the carbon dioxide rich bubbles from leaving the molten polymer solution and the sample pan.

Table 2. PCL−CO_2 Batch Foaming Experimental Parameters

T_{FOAM} (°C)	P_{IN} range (MPa)	T_{IN} (°C)	t_{FOAM} (s)
24	6.5−32	70	4
27	6.5−32	70	4
30	6.5−32	70	4

3.3. Batch Foaming Results. In batch foaming it is important to control the initial equilibrium temperature, T_{IN}, the initial pressure, P_{IN}, the foaming temperature, T_{FOAM}, and foaming time, t_{FOAM}, to obtain microcellular foams with controlled properties. During the equilibration step the polymer was maintained in its molten state at T_{IN} = 70 °C. Sorption equilibrium was obtained at the imposed initial pressure of $scCO_2$. The mixture was then rapidly cooled to the desired foaming temperature, T_{FOAM}, while maintaining a constant pressure in the system. The system was kept under these conditions for a few minutes to ensure the development of a uniform temperature distribution. No supersaturation was developed, since the solubility increases as the temperature decreases. The development of supersaturation and homogeneous nucleation of a foam structure was then induced by rapidly decreasing the pressure of the mixture to atmospheric pressure. The experimental conditions used in this study to produce the PCL foams with $scCO_2$ are summarized in Table 2. Due to the increase of solubility at lower temperatures, the CO_2 pressure should decrease as a consequence of increased CO_2 solubility after cooling. However, in view of the lower carbon dioxide diffusivity at the relatively low foaming temperatures, it is reasonable to assume that, during the few minutes allowed for temperature equilibration, no significant change of carbon dioxide concentration occurs in the polymer melt.

This laboratory-scale foaming procedure was adopted to mimic the processing conditions actually used to produce foams, where a molten polymer−gas mixture is formed at high temperature (e.g. in an extruder) and foaming occurs by depressurization at low temperature. The relatively low temperature used during foaming is required to permit immobilization of the foam through viscosity increase and, eventually, partial matrix crystallization after phase separation and cell formation.

Accurate control of the cooling rate following the saturation of the mixture was not possible. The experimental design allowed the attainment of the foaming temperature in the range 24−30 °C, however, to be reached in a few minutes.

3.4. Effects of Foaming Temperature and Initial Pressure on the Foam Structure. SEM photomicrographs of the PCL foams are presented in Figures 7 and 8. The samples have a uniform foam structure with a microporous core and apparently dense skin. The effect of foaming temperature on the foam structures is shown in Figure 7, where a marked difference is apparent

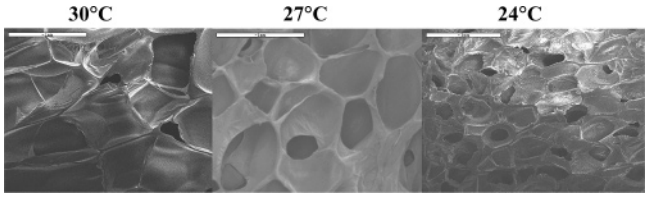

Figure 7. Scanning electron microscope micrographs of the cell structure of PCL foams obtained starting from CO_2/PCL solutions at 24, 27, and 30 °C subjected to rapid pressure decrease from 6.9 MPa to atmospheric pressure.

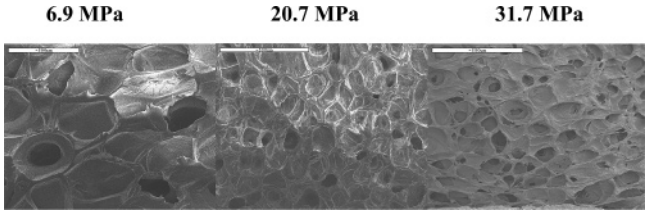

Figure 8. Scanning electron microscope micrographs of the cell structure of PCL foams obtained starting from CO_2/PCL solutions at 24 °C subjected to rapid pressure decrease from 6.9, 20.7, and 31.7 MPa to atmospheric pressure.

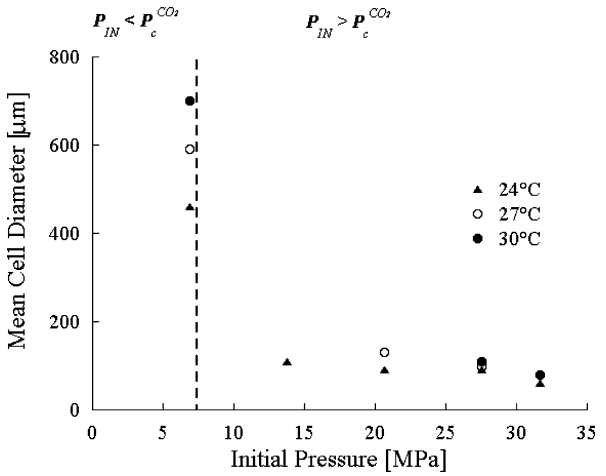

Figure 9. Effect of foaming temperature and initial pressure on the size of the foam cells. On the left side of the dotted line $P_{IN} < P_c^{CO_2}$, and on the right side $P_{IN} > P_c^{CO_2}$.

between the foam structures, generated at values of T_{FOAM} equal to 24, 27, and 30 °C and at P_{IN} equal to 6.9 MPa, in terms of number of cells per unit area and mean diameter of the cells. Moreover, various structures of the foams produced at values of P_{IN} equal to 6.9, 20.7, and 31.7 MPa at 24 °C are shown in Figure 8.

To analyze these effects, the mean diameter of the cells and the number of observed cells per unit area, in the pressure range 7−32 MPa for the three foaming temperatures, are plotted in Figures 9 and 10. The number of cells per unit area increases and the mean diameter of the cells decreases with increasing P_{IN} and decreasing T_{FOAM}. The dependence of the number of cells per unit area and the mean cell size on pressure appears to reach a plateau when $P_{IN} > P_c^{CO_2}$.

The number of bubbles formed during the batch foaming process and their mean size are determined by the competition between bubble nucleation and growth rates. If nucleation rate dominates, a larger number of cells and a smaller mean cell diameter is expected. The opposite holds if growth rate is higher.

In summary, foaming temperature influences several factors that, in turn, can have opposite effects on bubble

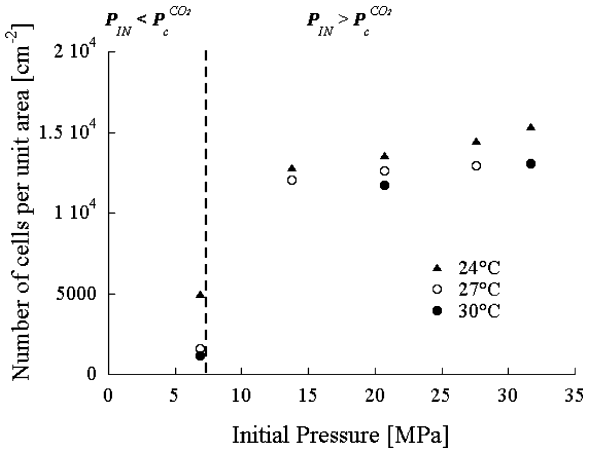

Figure 10. Effect of foaming temperature and initial pressure on the number of foam cells per unit area. On the left side of the dotted line $P_{IN} < P_c^{CO_2}$, and on the right side $P_{IN} > P_c^{CO_2}$.

nucleation and growth rate. As a consequence, the prediction of the effect of T_{FOAM} in the range 24−30 °C on the size and number of cells in the resulting foam is quite complicated. As a matter of fact, batch foaming experiments show that the competition between growth and nucleation rates give rise to the smallest cell size at the lowest foaming temperature (i.e. 24 °C).

If we fix T_{FOAM}, the dominating factor which determines the final cell size is P_{IN} or, more properly, the associated initial concentration of carbon dioxide. As the pressure increases, the supersaturation increases once depressurization is imposed. Consequently, the bubble diameter is expected to decrease while the number of bubbles is expected to increase as the initial pressure is raised. However, above a certain value of initial pressure (around 10.3 MPa) the initial concentration of CO_2 is found to be rather constant with pressure (see Figure 2). As a result, above a value of P_{IN} close to 10.3 MPa, the number and mean size of cells obtained by batch foaming become rather insensitive to initial equilibrium conditions.

4. Conclusions

Mass transport kinetics and sorption equilibria of CO_2 in PCL melts have been determined at 70, 80, and 90 °C at carbon dioxide pressures both below and above $P_c^{CO_2}$. The experimental sorption data were described by the Sanchez−Lacombe lattice model and the Peng−Robinson equation of state. The CO_2 mutual diffusivity has been determined as a function of concentration of dissolved CO_2. A steady increase with concentration up to a pressure of approximately 10 MPa, followed by a dramatic increase in the apparent effective diffusion coefficients at high pressure, was observed. This abrupt change can be attributed to the formation of a dispersed, fluid bubble phase, separate from the polymer−fluid solution. Interestingly, this phase separation phenomenon occurs in the regions of pressure/temperature where pure CO_2 compressibility also shows a maximum.

Biodegradable foams based on PCL were obtained with various cell densities and mean cell sizes, using a batch $scCO_2$ foaming process involving variation of initial pressure between 6.9 and 32 MPa and foaming temperature between 24 and 30 °C. The morphology of the resulting foams was related to the fundamental processes responsible for controlling both nucleation and growth of cells within the PCL foam. These fundamental

processes are additionally described in terms of the independently measured sorption equilibria and sorption kinetics measured and presented in the study.

Nomenclature

a = attraction parameter
b = van der Waals covolume
C = penetrant concentration
D = mutual diffusivity
$\bar{D}$ = average mutual diffusivity
f_1 = carbon dioxide fugacity in the pure gas phase
$G_1(T, P)$ = molar Gibbs free energy of carbon dioxide at T and P
$G_1^{IG}(T, P_{atm})$ = molar Gibbs free energy of ideal gas at T and $P = 1$ atm
$\bar{G}_1^{M}(T, P)$ = partial molar Gibbs free energy of carbon dioxide in the mixture at T and P
k = Boltzman constant
L = sample thickness
M_∞ = mass of carbon dioxide sorbed at equilibrium
M_t = mass of carbon dioxide sorbed at time t
M_1 = molecular weight of carbon dioxide
M_w = weight average molecular weight of PCL
P = pressure
P_{atm} = atmospheric pressure
P^* = characteristic pressure
ΔP^* = binary mixture parameter
P_{12}^* = binary mixture parameter
$\tilde{P}$ = reduced pressure of the PCL−CO_2 mixture
P_1^*, P_2^* = characteristic pressures (hypothetical cohesive energy density of a component in the *close-packed* state) of CO_2 and PCL
$\tilde{P}_1$ = reduced pressure of pure CO_2
P_c = critical pressure
$P_c^{CO_2}$ = CO_2 critical pressure
P_{IN} = initial pressure in the pressure vessel in a batch foaming experiment
R = gas constant
r_1^0 = number of lattice sites occupied by a carbon dioxide molecule in the pure gas state
r_1 = number of lattice sites occupied by a carbon dioxide molecule in the PCL−CO_2 mixture
T = absolute temperature
T^* = characteristic temperature of the PCL−CO_2 mixture
$\tilde{T}$ = reduced temperature of the PCL−CO_2 mixture
T_1^*, T_2^* = characteristic temperatures of CO_2, PCL
$\tilde{T}_1$ = reduced temperature of pure CO_2
T_c = critical temperature of carbon dioxide
T_{cry} = crystallization temperature of PCL
T_{FOAM} = foaming temperature
t_{FOAM} = foaming time, i.e., time elapsed for pressure drop
T_g = glass transition temperature of PCL
T_{IN} = initial temperature in a batch foaming experiment
T_m = melting temperature of PCL
V = volume
v = molar volume of carbon dioxide
v^* = average *close-packed* volume of a mer in the mixture
v_1^*, v_2^* = close packed volumes of a mer of CO_2 or of PCL in the pure state
Z = compressibility factor
X_1 = binary mixture parameter

Greek Letters

α = scaling factor
ϕ_1, ϕ_2 = close-packed volume fractions of CO_2, PCL
κ = characteristic constant in the definition of α
ρ^* = characteristic density (mass density in the *close-packed* state) of the PCL−CO_2 mixture
$\tilde{\rho}$ = reduced density of the PCL−CO_2 mixture
ρ_1^*, ρ_2^* = characteristic densities (mass densities in the *close-packed* state) of CO_2, PCL
$\tilde{\rho}_1$ = reduced density of pure CO_2
ω = acentric factor
ω_1, ω_2 = mass fractions of CO_2, PCL in the mixture
ψ = SL dimensionless interaction parameter

Superscripts

* = characteristic state
IG = ideal gas state
M = mixture

Subscripts

1, 2 = identification for CO_2, PCL
c = critical property
P_{atm} = properties and terms evaluated at $P = 1$ atm

Literature Cited

(1) Park, C. B.; Behravesh, A. H.; Venter, R. D. Low-density microcellular foam processing in extrusion using CO_2. *Polym. Eng. Sci.* **1998**, *38*, 1812.

(2) Martinache, J. D.; Royer, J. R.; Siripurapu, S.; Henon, F. E.; Genzer, J.; Khan, S. A.; Carbonell, R. G. Processing of polyamide 11 with supercritical carbon dioxide. *Ind. Eng. Chem. Res.* **2001**, *40*, 5570.

(3) Handa, Y. P.; Zhiyi, Z.; Wong, B. Solubility, diffusivity, and retrograde vitrification in PMMA-CO_2, and development of submicron cellular structures**.** *Cellular Polym.* **2001**, *20* (1), 1.

(4) Johnston, K. P., Penninger, M. L., Eds. *Supercritical Fluid Science and Technology*; ACS Symposium Series 406; American Chemical Society: Washington, DC, 1989 (developed from a symposium at the American Institute of Chemical Engineers Annual Meeting, Washington, DC, Nov 27−Dec 2, 1988).

(5) Goel, S. K.; Beckman, E. J. Nucleation and growth in microcellular materials: supercritical CO_2 as foaming agent. *AICHE J.* **1995**, *41*, 357.

(6) Shim, J.; Yates, M. Z.; Johnston, K. P. Polymer coating by rapid expansion of suspensions in supercritical carbon dioxide. *Ind. Eng. Chem. Res.* **1999**, *38*, 3655.

(7) Berens, A. R.; Huvard, G. S.; Korsmeyer, R. W.; Kunig, F. W. Application of compressed carbon dioxide in the incorporation of additives into polymers. *J. Appl. Polym. Sci.* **1992**, *46* (2), 231.

(8) Li, D.; Han, B. Impregnation of polyethylene (PE) with styrene using supercritical CO_2 as swelling agent and preparation of PE/polystyrene composites. *Ind. Eng. Chem. Res.* **2000**, *39*, 4506.

(9) Charpentier, P. A.; Kennedy, K. A.; DeSimone, J. M.; Roberts, G. W. Continuous polymerizations in supercritical carbon dioxide: chain-growth precipitation polymerizations. *Macromolecules* **1999**, *32*, 5973.

(10) Goel, S. K.; Beckman, E. J. Generation of microcellular polymeric foams using supercritical carbon dioxide I: Effect of pressure and temperature on nucleation. *Polym. Eng. Sci.* **1994**, *34* (14), 1137.

(11) Goel, S. K.; Beckman, E. J. Generation of microcellular polymeric foams using supercritical carbon dioxide. II: Cell growth and skin formation *Polym. Eng. Sci.* **1994**, *34* (14), 1148.

(12) Venerus, D. C.; Yala, N. Transport analysis of diffusion-induced bubble growth and collapse in viscous liquids. *AICHE J.* **1997**, *43* (11), 2948.

(13) Han, X.; Baxter, A. R.; Koelling, K. W.; Tomasko, D. L.; Lee, L. J. Influences of solubility and viscosity in the polystyrene/CO_2 microcellular foaming extrusion *Antec* **2002**, *60* (2), 1910.

(14) Di Maio, E.; Iannace, S.; Nicolais, L.; Flumerfelt, W.; Li, R. W. Structure optimization of PCL foams, by using mixtures of CO2 and N2 as blowing agents. *Polym. Eng. Sci.* **2005**, *45* (3), 432.

(15) Sanchez, I. C.; Lacombe, R. H. An elementary molecular theory of classical fluids. Pure fluids. *J. Phys. Chem.* **1976**, *80* (21), 2352.

(16) Sanchez, I. C.; Lacombe, R. H. Theory of liquid−liquid and liquid−vapor equilibriums. *Nature* **1974**, *252* (21), 381.

(17) Sanchez, I. C.; Lacombe, R. H. Statistical thermodynamics of fluids mixtures. *J. Phys. Chem.* **1976**, *80* (23), 2568.

(18) Sanchez, I. C.; Lacombe, R. H. Statistical thermodynamics of polymer solutions. *Macromolecules* **1978**, *11* (6), 1145.

(19) Peng, D. Y.; Robinson, D. B. A new two constant equation of state. *Ind. Eng. Chem., Fundam.* **1976**, *15* (1), 59.

(20) Cotugno, S.; Mensitieri, G.; Iannace, S.; Di Maio, E.; Ciardiello, C.; Nicolais, L. Sorption thermodynamics and mutual diffusivity of carbon dioxide in molten polycaprolactone. *Ind. Eng. Chem. Res.* **2003**, *42*, 4398.

(21) Kiszka, M. B.; Meilchen, M. A.; McHugh, M. A. Modelling high-pressure gas-polymer mixtures using the Sanchez-Lacombe equation of state. *J. Appl. Polym. Sci.* **1988**, *36*, 583.

(22) Hariharan, R.; Freeman, B. D.; Carbonell, R. G.; Sarti, G. C. Equation of state predictions of sorption isotherms in polymeric materials. *J. Appl. Polym. Sci.* **1993**, *50*, 1781.

(23) Vrentas, J. S.; Duda, J. L.; Ni, Y. C. Analysis of step-change sorption experiments. *J. Polym. Sci.: Polym. Phys. Ed*. **1977**, *15*, 2039.

(24) Crank, J. *The Mathematics of Diffusion*, 2nd ed.; Oxford University Press: Oxford, U.K., 1975.

(25) Pope, D. S.; Sanchez, I. C.; Koros, W. J.; Fleming, G. K. Statistical thermodynamic interpretation of sorption/dilation behavior of gases in silicone rubber. *Macromolecules* **1991**, *24*, 1779.

(26) Royer, J. R.; DeSimone, J. M.; Khan, S. A. Carbon dioxide-induced swelling of poly(dimethylsiloxane). *Macromolecules* **1999**, *32*, 8965.

(27) Koningsveld, R.; Stockmayer, W. H.; Nies, E. *Polymer Phase Diagrams: A Textbook*; Oxford University Press: New York, 2001.

(28) Wolf, B. A.; Geerissen, H. Pressure dependence of the demixing of polymer solutions determined by viscometry. *Colloid Polym. Sci*. **1981**, *259*, 1214.

(29) Melnichenko, Y. B.; Kiran, E.; Wignall, G. D.; Heath, K. D.; Salaniwal, S.; Cochran, H. D.; Stamm, M. Pressure- and temperature-induced transitions in solutions of poly(dimethylsiloxane) in supercritical carbon dioxide. *Macromolecules* **1999**, *32*, 5344.

(30) Sirard, S. M.; Ziegler, K. J.; Sanchez, I. C.; Green, P. F.; Johnston, P. K. Anomalous properties of poly(methyl methacrylate) thin films in supercritical carbon dioxide. *Macromolecules* **2002**, *35*, 1928.

(31) Sanchez, I. C.; Stone, M. T. In *Polymer Blends: Formulation*; Paul, D. R., Bucknall, C., Eds.; Wiley: New York, 2000; Vol. 1.

(32) Luna-Bárcenas, G.; Meredith, J. C.; Sanchez, I. C.; Johnston, K. P.; Gromov, D. G.; de Pablo, J. J. Relationship between polymer chain conformation and phase boundaries in a supercritical fluid. *J. Chem. Phys.* **1997**, *107* (24), 10782.

Received for review June 24, 2004
Revised manuscript received December 27, 2004
Accepted January 11, 2005

IE049445C